Structural Safety 99 (2022) 102255

Contents lists available at ScienceDirect

Structural Safety

journal homepage: www.elsevier.com/locate/strusafe

Next generation PBWE: Extension of the SAC-FEMA method to high-rise buildings under wind hazards

F. Petrini *, M. Francioli

Department of Structural and Geotechnical Engineering, Sapienza University of Rome, Rome, Italy

ARTICLE INFO

Keywords:
PBD
SAC-FEMA
Wind Engineering
Occupants' comfort

ABSTRACT

This paper proposes a method for the Performance-Based Wind Engineering (PBWE) of buildings by extending the well-established SAC-FEMA method originally implemented in seismic engineering for the evaluation of the mean annual frequency (MAF) of pertinent structural Limit States (LSs) in frame buildings. The development of such a method, that we will call the "SAC-FEMA WIND" method, implies the consideration of specific wind engineering peculiarities, like the classification of the across-wind response in two distinct regimes due to buffeting and vortex shedding phenomena, with the consequent adaption of the analysis procedures already defined for earthquakes to these two regimes. The method is then applied for the MAF evaluation of the occupants' comfort LS for a high-rise steel building: the SAC-FEMA WIND is calibrated by comparing the obtained results with those coming from a Monte Carlo numerical analysis. This allows the definition of appropriate analysis procedures and shows the reliability of the SAC-FEMA WIND in evaluating MAFs. The SAC-FEMA WIND can be viewed as a "next generation" method for PBWE, in the sense that, after years of developments of the PBWE in research, now simplified methods like the SAC-FEMA WIND are needed for the implementation in Standards and in the design practice of explicit probabilistic PBWE approaches.

1. Introduction

Performance-Based Wind Engineering (PBWE) is a general philosophy for the evaluation of structural performances under wind in probabilistic terms with design or assessment purposes ([1,2]). As recently well summarized in Bezabeh et al. ([3]), starting from its first formalization by a general procedure ([4]), PBWE has been deeply developed and improved during years regarding both the evaluation of Serviceability and Ultimate limit states (SLSs and ULSs) by different authors and for various structural typologies ([5–35]), and it is still an actual research topic ([36,37]).

It is not scope of this paper to provide an exhaustive state of the art regarding PBWE, for which the reader is addressed to [3], but it is important here to say that all the above-mentioned applications of PBWE are based on integral formulations for the evaluation of the occurrence of failure probabilities of the considered Limit States (LSs), (i.e., occurrence of the LSs in a certain reference period) meaning that a failure integral must be solved by conditional or unconditional approaches, as already defined for PBE under different hazards ([38,39]). Conditional approaches imply the evaluation of the structural fragility function and its convolution by the hazard curve, while the unconditional approach relies on the sampling of the structural response and in the evaluation of the failure probability integral by numerical estimations (e.g. Monte Carlo). In both cases, the explicit evaluation of the LSs failure probability implies the solution of an integral making the procedure not suitable to be implemented in Standards for explicit probabilistic PBWE.

Some authors proposed practical (non-integral) procedures for PBWE, but they are either focused on specific applications [40,41] or they address only specific aspects of the problem [42], or they do not explicitly evaluate the above mentioned occurrences of the considered limit states for a certain design configuration [43,44], while true probabilistic PBWE approaches would require such an evaluation.

In this view it is important to develop what can be referred as "next generation" PBWE approaches/methods, who allows the explicit evaluation of the LSs occurrences by an algebraic non-integral format. These next generation PBWE methods should be general (applicable to a broad band of LSs and structural typologies), and they should be affordable (while remaining probabilistically rigorous), in the sense that they must be as simple as possible (e.g., not requiring evaluation of failure

* Corresponding author at: Department of Structural and Geotechnical Engineering, Sapienza University of Rome, Rome, Italy.
E-mail addresses: francesco.petrini@uniroma1.it (F. Petrini), mattia.francioli@uniroma1.it (M. Francioli).

https://doi.org/10.1016/j.strusafe.2022.102255
Received 25 February 2022; Received in revised form 14 June 2022; Accepted 20 June 2022
Available online 2 July 2022

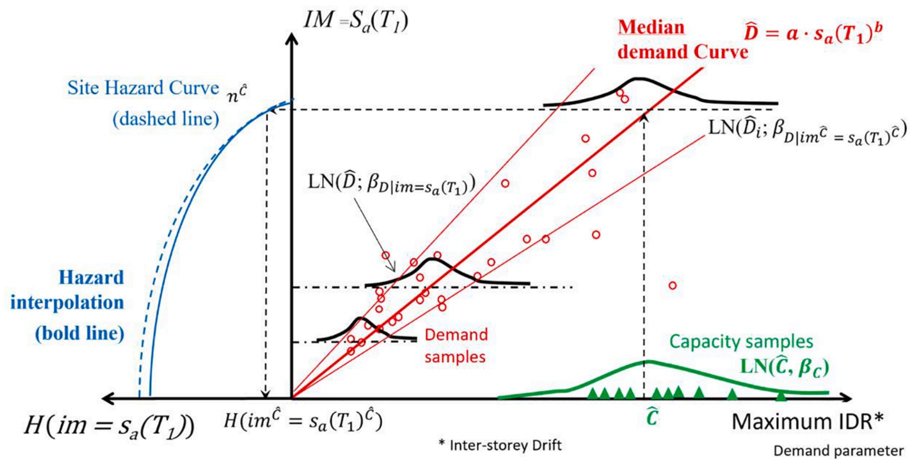

Fig. 1. SAC-FEMA method for earthquake engineering ().
adapted from [45]

integrals) for real-world design application; in other words, they must be suitable for being implemented in Standards. The research community working on PBWE is mature and well developed to pursue the goal of defining such these next generation methods, as already occurred in the Performance-Based Earthquake Engineering field [45].

Existing pre-Standards [46] and guidelines [47] for the implementation of PBWE in the practice, even if valuable since they correct define the framework, the models, and the LSs to be considered, they do not yet provide non-integral methods for explicit probabilistic evaluations.

The aim of this work is to contribute to the identification of a method that can be used in practical implementation of PBWE, and in Standards, for explicit evaluation of the mean annual frequency (MAF) for pertinent LSs. Therefore, the structural performances of a 3D steel high-rise building under wind loads is assessed by implementing the SAC-FEMA probabilistic approach already used in earthquake engineering [45] for the simplified evaluation MAF in frame buildings, and by specializing it for wind engineering purposes, something leading to the so called "SAC-FEMA WIND" method.

It has to say that, in addition to the above explained utility of the SAC-FEMA WIND, it will also allow to move towards a general approach for Performance-Based Multi-Hazard Engineering (PB-MH-E) for structures under wind and earthquake. To this regard it is worth noting that in case of wind and earthquake, the multi-hazard aspects do not focus on the simultaneous occurrence of the two hazards (which is known to be characterized by a very low probability), but rather on the correct design choices. In fact, as pointed out in [48], and with specific reference to the design of a structure which is sensitive both to wind and earthquake, the effects of the two different hazards on the structure can lead to conflicting design strategies (e.g. either reducing or increasing the flexibility). To deal with these conflicting strategies in an appropriate way, it is important that the methodological approaches and computational tools used in the performance analysis under the two different hazards, belong to a unified risk assessment/design framework, where the performances are expressed by the same metrics and languages for the two hazards ("unified framework problem"). The development of the SAC-FEMA WIND (which uses same performance metrics and performance evaluation tools of the SAC-FEMA for earthquakes) can then viewed as a first step toward the development of a true PB-MH-E, SAC-FEMA like method for buildings under the simultaneous consideration of wind and earthquake.

2. Materials and methods

2.1. SAC FEMA method for earthquakes

Originally, the SAC-FEMA approach has been proposed in Performance-Based Seismic Design (PBSD) of steel buildings [45], and it has been calibrated and gradually improved in years by a consistent number of literature papers (e.g. [49,50]).

The SAC-FEMA framework led to the simplified analytical calculation of the MAF for a certain LS, and it relies on the common scalar Demand Vs Capacity (*D* versus *C*) format, something that makes it suitable to be implemented in Standards for carrying out probabilistic performance analysis. Being all the uncertainties affecting the problem condensed in the *D*, the *C*, and in the hazard Intensity Measure parameter *IM* (the spectral acceleration at T_1, the fundamental period of the structure, i.e., $Sa(T_1)$, is often used as *IM* in case of seismic hazard), these three become the only explicit probabilistic terms of the analytical formulation.

The SAC-FEMA is based on some specific assumptions, regarding the probabilistic characterization of *D* and *C*, and regarding the interpolation of the hazard curve and the median demand, finally resulting in a simple algebraic expression of the MAF. By referring to the "2nd order" improved SAC-FEMA formulation proposed by Vamvatsikos (2014) [51], the assumptions can be summarized as below:

- first, the hazard curve is approximated by a second-order logarithmic interpolating law

$$H(im) = k_0 exp\left(-k_2 ln^2(im) - k_1 \ln(im)\right) \tag{1}$$

where k_0, k_1 and k_2 are constant coefficients, while *im* represents the sample scalar value of the Intensity Measure (*IM*) of the considered hazard;

- second, both *C* and *D* are assumed to follow lognormal distributions with median values $\hat{C}$ and $\hat{D}$ and dispersions β_C and $\beta_{D|im}$, being the *D* dispersion conditional to the *IM* value *im*. Namely $D = LN(\hat{D}, \beta_{D|im})$ and $C = LN(\hat{C}, \beta_C)$;
- third, the median *D* value is approximated by a power interpolating function

$$\hat{D} = a \bullet (im)^b \tag{2}$$

where *a* and *b* are constant coefficients.

It is worth noting that the hazard interpolation coefficients k_0, k_1 and k_2, are obtained by appropriate biased fitting of the seismic hazard curve

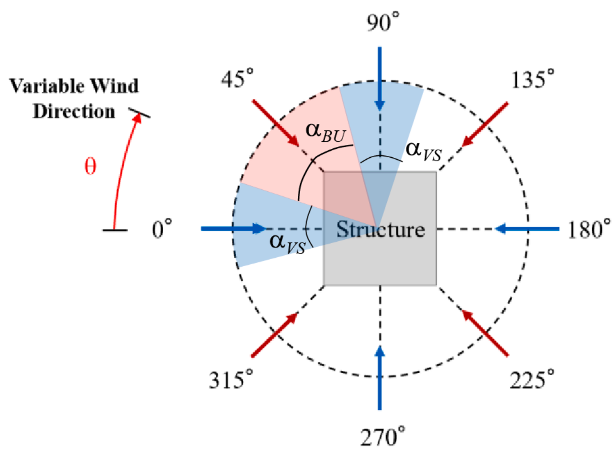

Fig. 2. Wind angles of incidence related to different aerodynamic regimes.

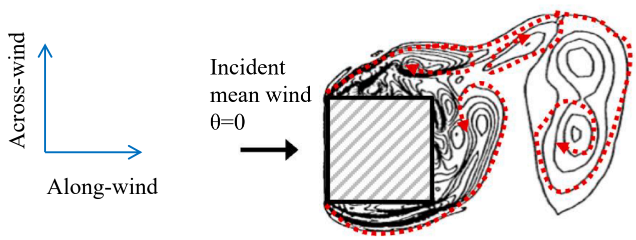

Fig. 3. *VS* aerodynamic regime (). adapted from [57]

at the site [52], while a and b and $\beta_{D|im}$ can be obtained by carrying out IDA [53], multiple-stripe [54] or Monte Carlo numerical analyses of the structural response, then by referring a and b to the median response curve at increasing *IM* values, and by quantifying $\beta_{D|im}$ by focusing on the scattering of structural response due both to the seismic signal (e.g. record to record variability) and to the uncertainties affecting the structural system (e.g. structural damping). Finally, $\widehat{C}$ and β_C are obtained by the statistical distribution of the capacity, which can be expressed in terms of limit forces (e.g. cross sections internal moments) or limit displacements (e.g. inter-storey drift IDR). It is worth noting that reliable values $\beta_{D|im}$ and β_C have been proposed in literature with reference to specific structural typologies under earthquakes [51].

Under the above-mentioned assumptions, the MAF of the specified LS can be evaluated by the expression in Eq (3):

$$\lambda_{PL} = \sqrt{\phi} k_0{}^{1-\phi} [H(im^{\widehat{C}})]^{\phi} exp\left[\frac{1}{2} q k_1^2 (\beta_C^2 + \phi \beta_D^2)\right] \quad (3)$$

where, in addition to the symbols introduced above we have,

$$q = \frac{1}{1 + 2k_2\beta_D^2/b^2} \quad (4)$$

$$\phi = \frac{1}{1 + 2k_2(\beta_D^2 + \beta_C^2)/b^2} \quad (5)$$

where $im^{\hat{C}}$ is the *IM* value for which $\widehat{D} = \widehat{C}$, and can be obtained from Eq (2) above as $im^{\hat{C}} = (\hat{C}/a)^{1/b}$. It is worth noting that in Equations (3–5) the conditioning of β_D from *im* has been eliminated by assuming a fixed and reasonable β_D value, for example one may choose to use a constant dispersion at the level of $IM = im^{\hat{C}}$ (i.e. $\beta_D = \beta_{D|im} = \beta_{D|im^{\widehat{C}}}$). The SAC-FEMA method can be efficiently summarized as shown in Fig. 1 for the case where the IDR is used as D parameter and the spectral seismic acceleration at the first mode period T_1 (i.e., $Sa(T_1)$) is used as *IM*.

2.2. SAC FEMA WIND method

In this section, the SAC-FEMA approach is extended to structural wind engineering problems, with specific focus on tall buildings. As already said in the introduction of the paper, the expression of the structural performances under wind in the same format/framework (called SAC-FEMA WIND in what follows) used for earthquake is crucial both for practical implementation of PBWE and for PB-MH-E purposes.

Obviously, the SAC-FEMA WIND approach must be specialized to consider specific peculiarities of structural wind engineering problems. In this view, one of the most relevant aspects to consider in the structural response of tall buildings under wind, is the strong dependence of the aerodynamics and of the resulting structural D, from the incident wind direction θ relatively to the structure [55]. Such a strong dependence of the action/demand from the direction is not generally present in earthquake engineering and then is not explicitly taken into account in the original SAC-FEMA. Specifically, in a square floor plan prismatic building, wind incident angles corresponding to orthogonal directions with respect to building façades, namely $\theta = 0°; 90°; 180°; 270°$ in Fig. 2, are related to square-shape bluff-body aerodynamics, then implying predominant vortex shedding effects (*VS*), with potential lock-in phenomenon leading to large floor displacements and accelerations in the across-wind direction (as qualitatively shown in Fig. 3). On the contrary, edge-incident winds, namely $\theta = 45°; 135°; 225°; 315°$ in Fig. 2, are related to rhomboidal-shape aerodynamics, which is usually not associated to relevant *VS* effects, or to relevant across-wind structural responses. Intermediate situations, e.g $0° < \theta < 45°$, can be associated to the gradual transition between the two aerodynamic regimes.

For this reason, it is appropriate to treat the wind-induced demand in the across-wind direction as generated mainly by two distinct response regimes depending on the wind incident angles: i) those potentially characterized by the *VS* and; ii) those induced by the intrinsic atmospheric turbulence without any significant *VS* effect (buffeting regime *BU*).

To be more specific in case of square buildings, and by referring to the Fig. 2, in the SAC-FEMA WIND approach, the structural response under wind loads is assumed to occur in *VS* regime when the θ belongs to sectors of amplitude α_{VS} centered on the previous specified façade-orthogonal incident angles, and related to square-shape bluff-body aerodynamics ($\theta = 0°; 90°; 180°; 270°$ in Fig. 2), while the structural response is assumed to occur in *BU* regime for incident wind sectors of amplitude α_{BU} centered on angle values related to rhomboidal-shape aerodynamics ($\theta = 45°; 135°; 225°; 315°$ in Fig. 2).

The assumed amplitude α_{VS} and α_{BU} should be calibrated to statistically reproduce the building response samples population under a significant number of wind directional events. As a preliminary indication, it can be said that the amplitude of *VS* sectors α_{VS} is expected to be lower than the one of the buffeting sectors α_{BU}.

It is important to point out that:

- in general *VS* and *BU* regimes can be present at all incident angles with different intensity, then "*VS*" and "*BU*" must be intended as "predominant vortex shedding" and "predominant buffeting" effects;
- the occurring of *VS* or *BU* aerodynamic regimes depends mainly on the building geometry/aerodynamic shape given at a certain incident wind direction, and the identification of the related incidence sectors in the wind rose has to be made by appropriate wind tunnel tests or computational fluid dynamic analyses [56]. It is known that for square buildings, these incidence wind sectors are those shown in Fig. 2.

With these specifications, the SAC-FEMA format can be applied to tall buildings under wind loads by differentiating between the *VS* and *BU* aerodynamic regimes, and then by formulating the analytical expression of the MAF for the two regimes separately, something identified by appropriate subscript indications in equations that follow (e.g.

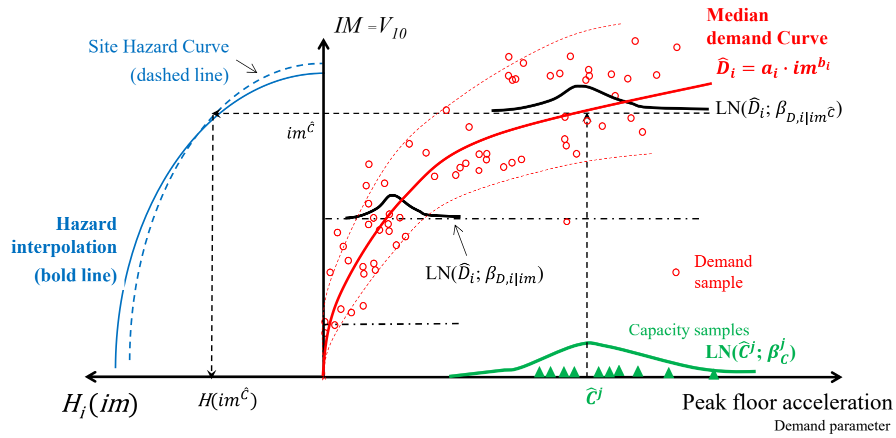

Fig. 4. SAC-FEMA WIND schematic representation.

the subscript i, with $i = VS$ or BU).

Coherently with the original SAC-FEMA, in the SAC-FEMA WIND it is assumed that: a) D follows the lognormal distribution for both aerodynamics regimes, then $D_i = \mathrm{LN}(\widehat{D}_i, \beta_{D,i})$, that is $D_{VS} = \mathrm{LN}(\widehat{D}_{VS}, \beta_{D,VS})$, $D_{BU} = \mathrm{LN}(\widehat{D}_{BU}, \beta_{D,BU})$ for $i = VS$ or BU respectively and; b) the median demands for the two cases are interpolated by power law functions $\widehat{D} = a_i \bullet (im)^{b_i}$ with $i = VS$ or BU.

Regarding the IM, the V_{10} (10-minutes average mean wind speed at 10 m height) is identified as the appropriate (structure independent) wind intensity parameter and it is assumed to follow a Weibull probability distribution on an annual time scale [6]. The V_{10} Weibull distribution is characterized by the shape and scale parameters values that are conditional to the wind angle of incidence θ. Consequently, to maintain the differentiation between the VS and BU demand regimes, the hazard curve should be also differentiated in two cases: one associated to the VS incidences and the other associated to the BU incidences, both obtained as the weighted average of the Weibull distributions associated to the pertinent incident wind sectors (as identified in Fig. 2).

As for the earthquake case, the hazard is interpolated by a second order function having the shape in Eq (1), but the interpolations coefficients are specific for the VS and BU cases, resulting in two interpolating curves for the hazard:

$$H_i(im) = k_{0,i} exp\left(-k_{2,i} ln^2(im) - k_{1,i} ln(im)\right) \tag{6}$$

where $i = VS$ or BU, and $k_{0,\,i}$, $k_{1,\,i}$ and $k_{2,\,i}$ are constant interpolation coefficients.

Focusing on C, of course, it is not differentiated between the two considered demand regimes, but it is specific of the threshold value associated with the considered LS, which can be indicated by the superscript j (i.e., C^j). For example, it is expected that one of the design-driving performance requirements for tall building under wind is the SLS related to the discomfort of the building occupants due to the perception of the building motion, for which the relevant D parameter is the peak top floor acceleration induced in across-wind direction a_{peak_L} [7,10]. In this case $\widehat{C}$ is represented by the median value of the floor acceleration associated to the motion perception for a certain percentage N_p of the floor occupants, which is differentiated between offices (OFF) and apartments (APT) building occupation [47]. By assuming that C follows the lognormal distribution then, it can be written: $C^j = \mathrm{LN}(\widehat{C}^j, \beta_C^j)$ with $j = APT$ or OFF.

With these premises, the SAC-FEMA WIND, when used in evaluating the MAF for buildings occupants to feel vibration-induced discomfort, assumes the following general formulation:

$$\lambda_i^j = \sqrt{\phi}\, k_{0,i}{}^{1-\phi_i^j}\left[H_i\left(im^{\widehat{C}^j}\right)\right]^{\phi_i^j} \bullet exp\left[\frac{1}{2} q_i k_{1,i}^2 \left(\beta_C^{j\,2} + \phi_i^j \beta_{D,i}^2\right)\right] \tag{7}$$

$$q_i = \frac{1}{1 + 2k_{2,i}\beta_{D,i}^2 \big/ b_i^2} \tag{8}$$

$$\phi_i^j = \frac{1}{1 + 2k_{2,i}\left(\beta_{D,i}^2 + \beta_C^{j\,2}\right) \big/ b_i^2} \tag{9}$$

With $i = VS$ or BU; $j = APT$ or OFF. For each sub-case identified by i and j, the symbols in Eqs (7–9) have the same meaning of those already defined for earthquakes in Eqs. (3–5). For example, the above equations for the MAF of discomfort in apartment buildings due to the vortex shedding becomes:

$$\lambda_{VS}^{APT} = \sqrt{\phi}\, k_{0,VS}{}^{1-\phi_{VS}^{APT}}\left[H_{VS}\left(im^{\widehat{C}^{APT}}\right)\right]^{\phi_{VS}^{APT}} \bullet exp\left[\frac{1}{2} q_{VS} k_{1,VS}^2 \left(\beta_C^{APT\,2} + \phi_{VS}^{APT} \beta_{D,VS}^2\right)\right] \tag{10}$$

$$q_{VS} = \frac{1}{1 + 2k_{2,VS}\beta_{D,VS}^2 \big/ b_{VS}^2} \tag{11}$$

$$\phi_{VS}^{APT} = \frac{1}{1 + 2k_{2,VS}\left(\beta_{D,VS}^2 + \beta_C^{APT\,2}\right) \big/ b_{VS}^2} \tag{12}$$

Given the occupancy j of the building (APT or OFF), and if λ_{VS}^j and λ_{BU}^j are calculated by equations (7–9), the total resulting MAF for the occupant discomfort will be obtained as:

$$\lambda^j = \frac{\left(n_{VS}\,\lambda_{VS}^j + n_{BU}\,\lambda_{BU}^j\right)}{N_{TOT}} \tag{13}$$

Where n_{VS} and n_{BU} are the annual probabilities at the site for the wind angle of incidence to fall in the sector associated to VS or to BU respectively, and N_{TOT} is the sum of the two ($N_{TOT} = 1$ if the VS and BU sectors together cover the whole wind rose).

The points to be still addressed here, regard the analysis procedures to implement for the evaluation of several parameters in the SAC-FEMA WIND equations. This is discussed in the next section with specific focus on the above-mentioned occupants' comfort SLS.

2.3. Analysis procedures

The application of the proposed SAC-FEMA WIND method implies the development of some specific analysis steps for the evaluation of the

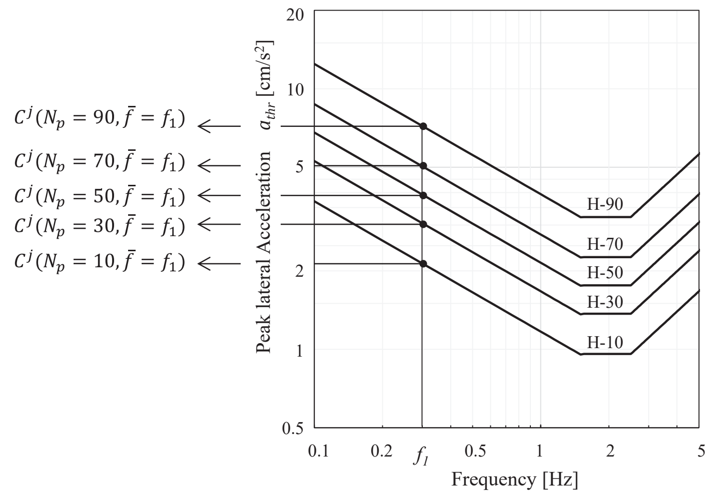

Fig. 5. Vibration perception thresholds.
Adapted from [70]

Table 1

Different literature values for $a_{threshold}$ (cm/s^2) and calculation of $\widehat{C}^{APT}$ and β_C^{APT} for the vibration frequency $\bar{f} = 0.187$ Hz.

	Ref No	Reference	*Np* [%]						
			2	5	10	25	50	75	95
a_{thr} [mm/s^2]	1	Chen, Robertson (1972) [63]	19.02	23.59	28.56	39.32	56.08	79.99	133.31
	2	ISO 6987 (1984) [64]	–	–	–	–	–	–	126.94
	3	Melbourn, Cheung (1988) [65]	–	–	–	–	–	–	107.91
	4	Tamura et al. (1988) [66]	27.57	32.31	37.21	47.10	61.21	79.54	115.94
	5	NBR6123 (1988) [67]	–	–	–	–	–	61.31	–
	6	Isyumov (1993) [68]	–	–	–	–	–	68.67	–
	7	Kanda et al. (1994) [69]	18.46	22.84	27.59	37.83	53.72	76.28	126.33
	8	AIJ (2004) [70]	19.00	23.00	27.05	35.20	49.71	65.00	112.00
	9	Tamura et al. (2006) a [71]	18.95	23.31	28.02	38.12	53.65	75.51	123.45
	10	Tamura et al. (2006) b [71]	21.17	25.38	29.81	39.00	52.58	70.89	108.95
	11	Tamura et al. (2006) c [71]	18.98	23.03	27.34	36.42	50.09	68.88	108.94
	12	Tamura et al. (2006) d [71]	21.58	25.41	29.37	37.41	48.95	64.05	94.31
	13	Tamura et al. (2006) e [71]	23.15	27.10	31.17	39.38	51.07	66.22	96.24
	14	ISO 10,137 (2007) [72]	–	–	–	–	–	–	112.00
	15	Burton et el. (2007) a [73]	–	–	–	–	–	–	136.36
	16	Burton et el. (2007) b [73]	–	–	–	–	–	–	158.24
	17	Sarkisian (2012) [74]	–	–	–	–	–	68.67	–
	18	Ferrareto et al (2014) [75]	–	–	–	–	–	–	97.12
$\widehat{C}^{APT}(N_p, 0.187)$[mm/s^2] Eq. (14)			20.19	24.30	28.62	37.62	51.40	69.44	112.00
$\beta_C^{APT}(N_p, 0.187)$ Eq. (15)			0.132	0.113	0.099	0.082	0.070	0.087	0.143

Note 1: when not available, *Np* has been assumed as consistent with those declared by other considered references
Note 2: when the a_{thr} has not been associated by authors to a specific vibration frequency, it has been considered valid for any considered frequency

hazard and the median demand interpolation parameters, and for the definition of the demand and capacity dispersions.

First, the sectors amplitude α_{VS} and α_{BU} should be defined to identify which incident wind directions θ are associated to *VS* or *BU*. By referring to the aerodynamics of a square-plan building (Fig. 3 and text herein) the *VS* sectors should have a maximum amplitude $\alpha_{VS} = 45^\circ$ and should be centered on the incidences orthogonal to the building-façades (for example a *VS* sector can be $-22.5 < \theta < +22.5$, that is $\alpha_{VS} = 45^\circ$). Experience suggests that, as already said, an appropriate α_{VS} value for square buildings should be$<45^\circ$ since the *VS* rapidly vanishes with the incidences moving away from orthogonal-to-façades cases ([6,58]). The influence of the assumed value for α_{VS} on the MAF is investigated in Appendix A with reference to the case-study structure (square floor building), here it can be anticipated that a suggested value for α_{VS} is 30°.

The *VS* and *BU* hazard curves can be then identified from the site climatology and each one can be interpolated by Eq. (6). To maximize the interpolation efficiency, some biased fit, as defined for earthquakes in [51], can be implemented.

On another side, the median demand under increasing *IM* values must be evaluated and successively interpolated by a power function like the one in Eq. (2). The *D* evaluation step needs to be made by the avail of the structural analysis: if for example a Monte Carlo or Multiple Stripe analysis (where the uncertain parameters vary by following appropriate probabilistic distributions is carried out), as a result several demand samples will be available on the *D-IM* plane as shown in Fig. 4. This representation allows for the estimation of both the median demand curve and its dispersion as shown in the Figure. Alternatively, if the demand dispersion is known or it is assumed from the literature, deterministic structural incremental (i.e. at increasing *IM* values) analyses can be conducted by considering the median values of uncertain parameters other than *IM* to evaluate the median demand curve. As specified in the conclusion of the paper, further research is needed to

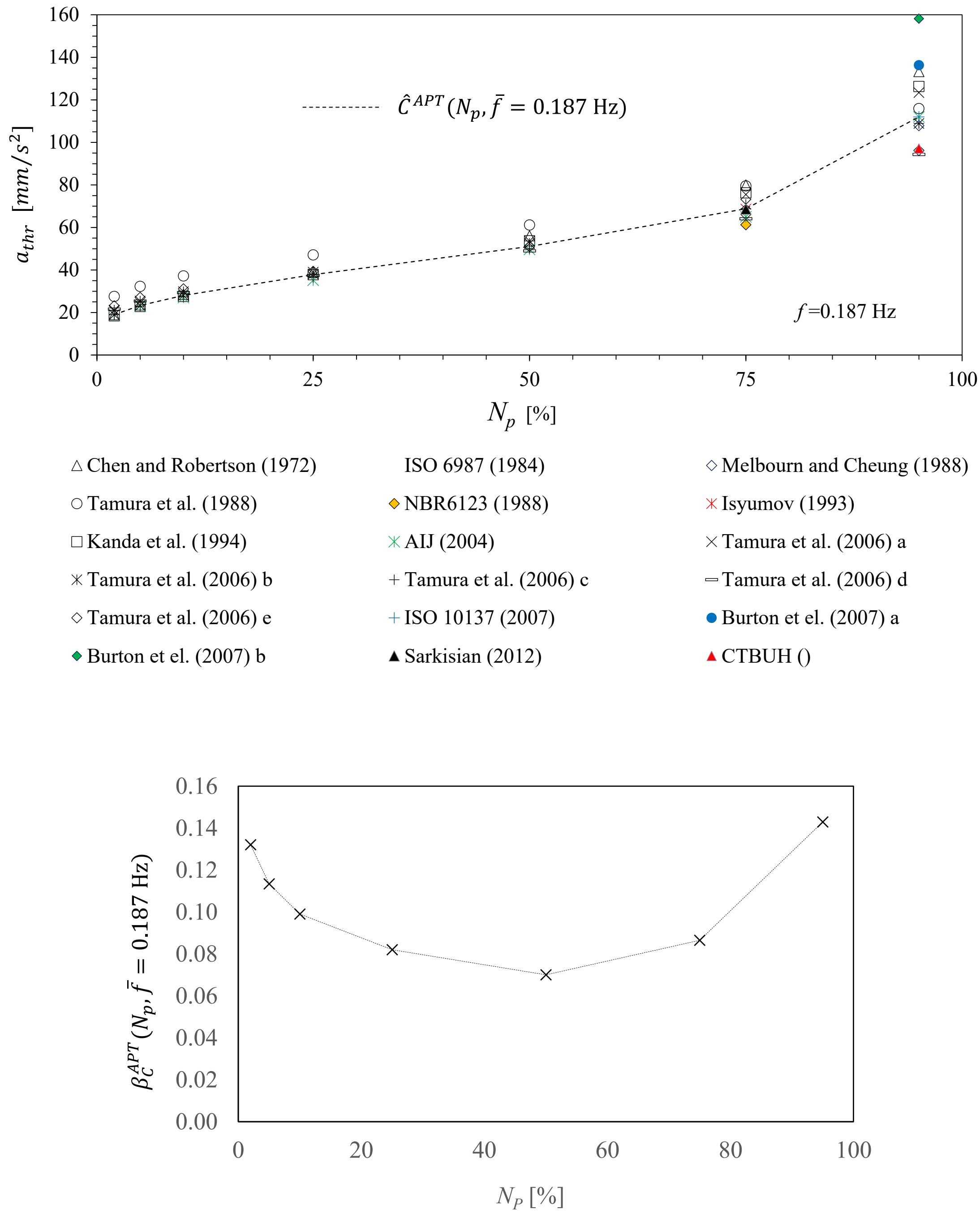

Fig. 6. Evaluation of the median and the dispersion values of the capacity. Reference value of the capacity taken from the literature and median estimation (top) and capacity dispersion (bottom).

produce a literature regarding the demand dispersion, and at the current state, the authors of this paper suggest the adoption of valued between 0.2 and 0.5, based on the expected demand dispersion for the specific problem. Another point regarding the median demand interpolation, can be understood by comparing the earthquake and wind cases of Figs. 1 and 4 respectively: it is noted from Fig. 4 that the increasing rate of the $\hat{D}$ curve for wind at high *IM* values is represented as larger than the one in earthquake engineering, as usually occur [59]. This is something that requires the implementation in the SAC-FEMA WIND, of some appropriate interpolation strategies for the median demand in order to guarantee a good MAF estimation. This point will be discussed in the application section.

On the *C* side, the selection of appropriate techniques for the evaluation of the median and the dispersion values, is strictly related to the considered LS. Focusing on the occupants' comfort SLS, as already said, the *C* will be a (frequency-dependent) peak floor acceleration threshold a_{thr} that, if exceeded, implies that a certain percentage N_p of the floor occupants perceives the building motion. The $\hat{C}^j$ and β_C^j values will then depends on the chosen N_p percentage and on the main vibration frequency $\bar{f}$ (usually assumed as coincident to the building first natural frequency in the vibration direction, that is $\bar{f} = f_1$). To determine $\hat{C}^j$ and β_C^j, reference can be made to the literature works regarding the topic of motion-induced discomfort (e.g. [60–75]): for each considered

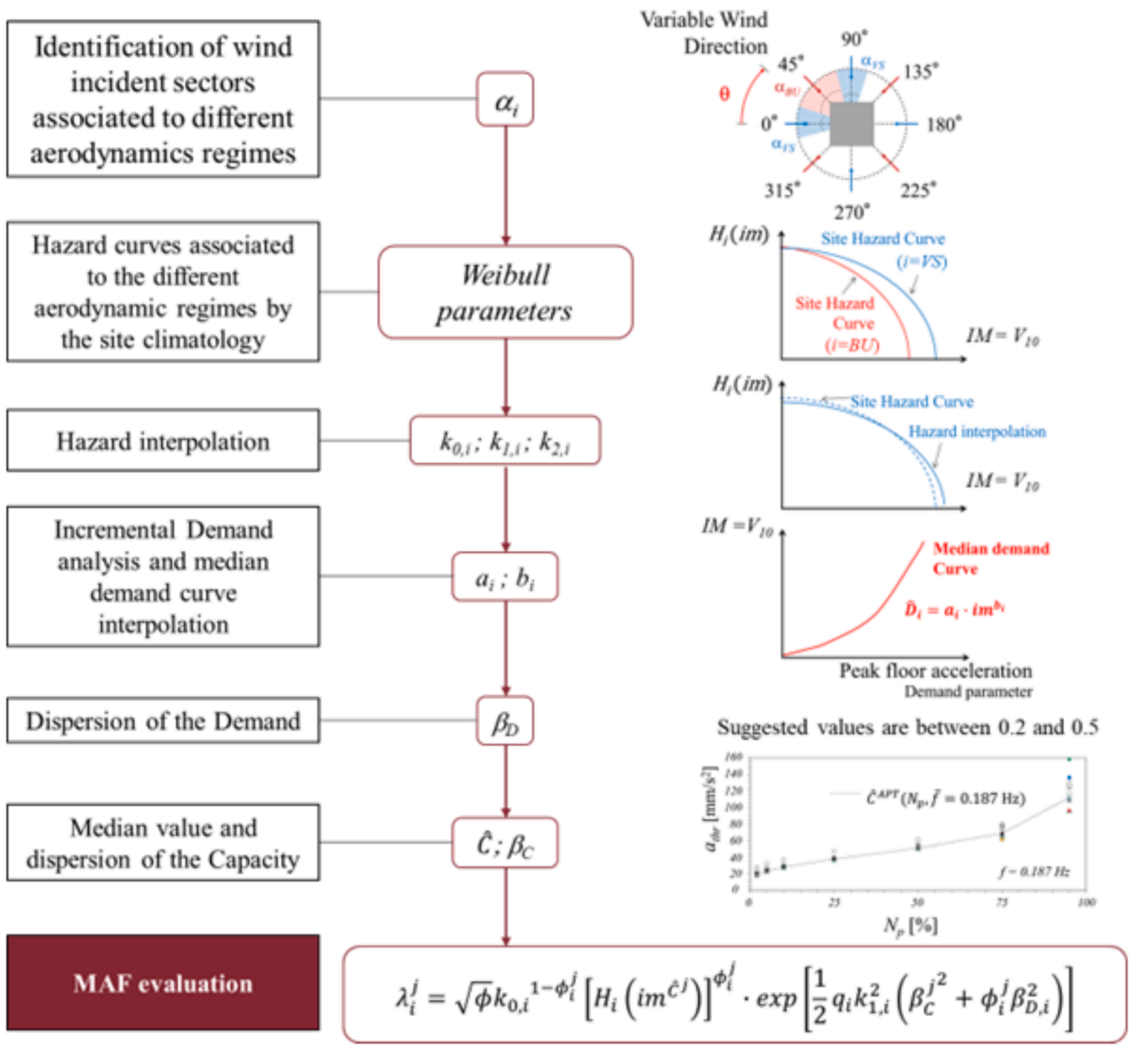

Fig. 7. SAC-FEMA WIND flowchart.

literature reference, the data herein reported about the joint values of N_p, $\bar{f}$ and a_{thr} can be collected in order to obtain a set of frequency-dependent perception threshold curves as the one shown in Fig. 5 and extracted from the AIJ Guidelines (2004) [70]. By entering in the graph of Fig. 5 with the first vibration frequency of the building f_1, the corresponding a_{thr} indicated by different curves can be interpreted as those associated in the literature reference with the N_p percentage at $\bar{f} = f_1$, where N_p is indicated above the curves.

By collecting the same data from a number n_{ref} of different reference works, the $\widehat{C}^j$ and β^j_C values associated to certain N_p, and a certain $\bar{f}$ value can be estimated respectively as median and logarithmic standard deviation ([76,77]) of the a_{thr} values obtained by the different references.

$$\widehat{C}^j(N_p,\bar{f}) = median\{a_{thr\_ref\_x}(N_p,\bar{f})\} \quad (14)$$

$$\beta^j{}_C(N_p,\bar{f}) = stdev\{\ln[a_{thr\_ref\_x}(N_p,\bar{f})]\} \quad (15)$$

where $x = 1,\ldots, n_{ref}$, being n_{ref} the total number of selected reference papers for data extraction.

The procedure described above for $\beta^j{}_C(N_p,\bar{f})$ estimation and equations (14) and (15) have been implemented here with demonstrative purposes for the case$N_p[\%] = 2, 5, 10, 25, 50, 75, 95$ and $\bar{f} = 0.187$ Hz (which is the first vibration frequency f_1 of the case-study building used for the application in the next section), and $j = APT$. The considered literature references and the a_{thr} values are reported in Table 1 together with the obtained $\widehat{C}^{APT}$ and β_C^{APT}, while they are graphically represented in Fig. 6.

When all the necessary parameters are quantified, the MAF can be evaluated by equations (7–9; 13). The whole procedure for the SAC-FEMA WIND method for the MAF evaluation of the occupant comfort LS is represented in Fig. 7.

3. Results: Application to a High-Rise building

3.1. Description of the case study

The proposed SAC-FEMA WIND method is applied to a 74-storey steel high-rise building already studied by one of the authors in previous papers [6]. The building structure is in steel, it has a 50x50m square plan and it is 305 m high, it is located in Orlando, Florida (US), all the details regarding the hazard characterization (Weibull parameters for the wind velocity along different sectors of the wind rose), and the cross section of the structural elements are provided in Ciampoli & Petrini (2012) [6], the structural FE model of the building is developed in ANSYS® and it is shown in Fig. 8. The first vibration frequency of the

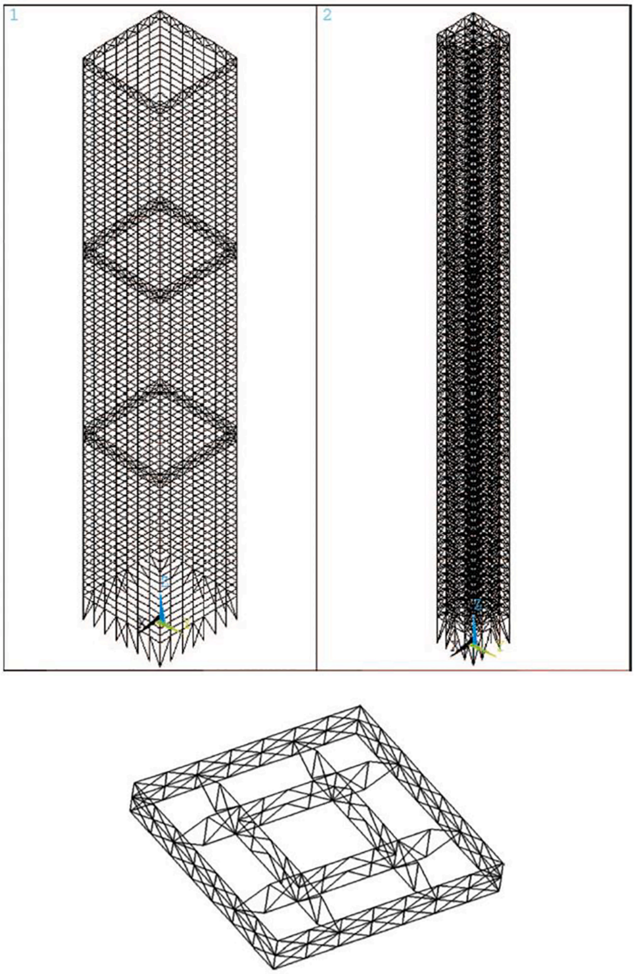

Fig. 8. FE model of the structure. Top: external frame and core; bottom: outrigger trusses.

building in across and along wind directions is $f_1 = 0.1873$ Hz.

The structural response of the building is evaluated only in the across wind direction (then having zero-mean value) and is obtained in the frequency domain by a Power Spectral Density (PSD) analysis [6,7,27] by applying along and across wind force spectra at each floor of the building.

The demand parameter for comfort performances evaluation is the peak top floor acceleration induced in across-wind direction $D = a_{peak\_L}$, obtained by evaluating the response's variance as the area underpinned by the acceleration PSD response function of the top floor master node, and then by applying the Davenport's peak factor.

$$g_r = \sqrt{2\,ln(\eta\,T_{wind})} + \frac{0.577}{\sqrt{2\,\ln(\eta\,T_{wind})}} \tag{16}$$

where η is the cycling rate of the effective frequency of the response, assumed equal to the first natural frequency f_1 of the structure; T_{wind} is the time interval over which the maximum response is evaluated. In this case, $f_1 = 0.1873$ Hz, while $T_{wind} = 3600$ s; the nominal value of the peak factor is $g = 3.769$. The use of the Davenport's peak factor in Eq. (16) may lead to conservative peak evaluations if *VS* dominates the response since the Davenport's formula does not take into account for the badwidth of the response stochastic processes. Alternative formulations which take into account the effect of the bandwidth are available in literature (e.g. [78,79]) and have been explored by the authors in previous works ([6]), but they have not been implemented here to avoid additional analytical complications. It is important to say that the use of the Davenport's peak factor does not compromise the generality of the proposed SAC-FEMA WIND method.

The building is characterized by a mean damping ratio $\xi = 0.008$, and by a bulk density $bulk = 111.71$ Kg/m^3, leading to a mass per unit of length $m = bulk \cdot B \cdot B = 111.71 \cdot 50 \cdot 50 = 279275$ Kg/m. By assuming $\rho = 1.25$ Kg/m^3 for the air density, the Scruton number for the building is $Sc = 9$ as evaluated by Eq (17), which indicates that the building is sensitive to the *VS* induced response [47].

$$S_C = \frac{4\pi \bullet m \bullet \xi}{\rho \bullet B^2} \tag{17}$$

In order to evaluate the performances of the building for comfort, the demand in terms of peak accelerations obtained by the analyses, are compared with the capacity in terms of acceleration perception thresholds, whose median and dispersion values are defined by the procedure described above for $j = APT$ (Table 1 and Fig. 6) and by considering $Np = 90\%$, resulting in $\widehat{C}^{APT} = 0.1012$ m/s^2 and$\beta_C^{APT} = 0.143$. For what concerns the $j = OFF$ building occupation, the median capacity is obtained by the CNR-DT guidelines ([47]), reporting $\widehat{C}^{OFF} = 0.153$ m/s^2, while the capacity dispersion is reduced in offices with respect to apartments. The decreasing of the capacity dispersion in office with respect to apartments is due to the consideration that, as reported in the relevant literature ([60,61,62,71,73]), such a dispersion depends from many factors like the variety of the occupants' tasks or ages. Since it can be reasonably assumed that both tasks and ages of offices' occupants are narrowed with respect to apartments, the authors assumed$\beta_C^{OFF} = 0.8 \cdot \beta_C^{APT}$, resulting in the value$\beta_C^{OFF} = 0.114$.

4. Reference results by Monte Carlo analysis

A Monte Carlo (MC) analysis including a total of 5000 samples has been first carried out to evaluate some reference values of the failure probabilities to be used in the calibration of the SAC-FEMA WIND.

In the MC analysis, while the along-wind floor force spectra are evaluated by the Solari spectrum, in the across-wind direction, depending to the wind angle of incidence, the Solari [47], the Liang [80] wind spectrum, or a combination of the two are implemented for *BU* ($\theta = 45°; 135°; 225°; 315°$), *VS* ($\theta = 0°; 90°; 180°; 270°$), or transition (e.g. $0° < \theta < 45°$) wind regimes respectively. The two across-wind spectra are then combined by a scalar a coefficient $c(\theta)$ which, for the considered case of a square prismatic building, assumes a unitary value when the wind impacts orthogonally to one of the façades ($\theta = 0°; 90°; 180°; 270°$), while it assumes a null value in the event that the wind impacts on a corner of the building ($\theta = 45°; 135°; 225°; 315°$). The resulting expression of the diagonal terms of the across-wind floor forces PSD matrix at the height z_l with respect to the ground when the frequency n is expressed in Hz is:

$$S^{TOT}{}_{F_{v_l}F_{v_l}}(n, z_l, z_l) = c(\theta) \bullet S'{}_{F_{v_l}F_{v_l}}(n, z_l, z_l) + (1 - c(\theta)) \bullet S_{F_{v_l}F_{v_l}}(n, z_l, z_l) \tag{18}$$

In equation (18) $S'{}_{F_{v_l}F_{v_l}}(n, z_l, z_l)$ is the Liang spectrum given by

$$S'{}_{F_{v_l}F_{v_l}}(n, z_l, z_l) = \frac{\sigma(z_l)^2}{n}\left[\frac{\overline{A}\,H(C_1)\overline{n}^2}{(1-\overline{n}^2)^2 + C_1\overline{n}^2} + \frac{(1-\overline{A})\sqrt{C_2}\,\overline{n}^3}{1.56\left[(1-n^2)^2 + C_2\overline{n}^2\right]}\right] \tag{19}$$

In which.

$$\sigma(z_j) = \frac{1}{2}\rho\, V_m^2(z_j)\mu_{c_L} B\, \Delta z_l \tag{20}$$

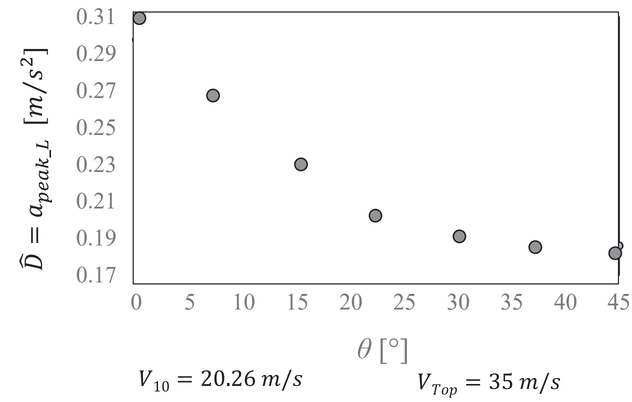

Fig. 9. Top floor across-wind peak accelerations for the building at a constant value of V_{10} and different θ values.

Table 2
Monte Carlo analysis. Considered uncertain parameters and probability distributions.

Parameter	Type of distribution and values type	values
V_{10} [m/s]	Weibull	shape and scale factors depend on θ
θ [deg]	Derived by NIST wind speed database	
z_0 [m]	Lognormal	μ_{z0} and σ_{z0} depend on θ
ξ[-]	Lognormal	$\mu_\xi = 0.008$; $COV_\xi = 0.3$
C_L	Gaussian	μ_{CL} depends on θ; $COV_{CL} = 0.05$–0.1 depending on V_{10}

$$\overline{A} = \frac{H}{\sqrt{S}}\left[-0.118\left(\frac{D}{B}\right)^2 + 0.358\left(\frac{D}{B}\right) - 0.214\right] + \left[0.066\left(\frac{D}{B}\right)^2 - 0.26\left(\frac{D}{B}\right) + 0.894\right] \tag{21}$$

$$\mathrm{H}(C_1) = 0.179\, C_1 + 0.65\sqrt{C_1} \tag{22}$$

$$C_1 = \frac{\left[0.47(D/B)^{2.8} - 0.52(D/B)^{1.4} + 0.24\right]}{\left(H/\sqrt{S}\right)} \tag{23}$$

In equations (18–23), Δz_l indicates the tributary height for the floor l, i.e. half upper interstorey plus half lower interstorey, B is the width of the building, μ_{c_L} is the mean lift coefficient, $\overline{A}$ is the power-assignation coefficient, D is the length of the building (=B for the case study), S is the cross-sectional area of the floor, H is the total height of the building, $\overline{n} = \frac{n}{n_s}$ while $n_s = \frac{S_t V_m(z_l)}{B}$ is the frequency of vortex shedding determined by the Strouhal number S_t, and C_2 is equal to 2.

In equation (18) $S_{F_{v_l}F_{v_l}}(n, z_l, z_l)$ is the floor force spectrum obtained by the Solari wind turbulence spectrum $S_{v_l v_l}(n, z_l, z_l)$ given by.

$$S_{F_{v_l}F_{v_l}}(n, z_l, z_l) = \left(\mu_{c_L} A_T \rho\right)^2 \bullet S_{v_l v_l}(n, z_l, z_l) \tag{24}$$

where.

$$\frac{n S_{v_l v_l}(n, z_l, z_l)}{\sigma_v^2(z)} = \frac{9.434\, n_v}{\left[1 + 14.151\, n_v^2(z_l)\right]^{5/3}} \tag{25}$$

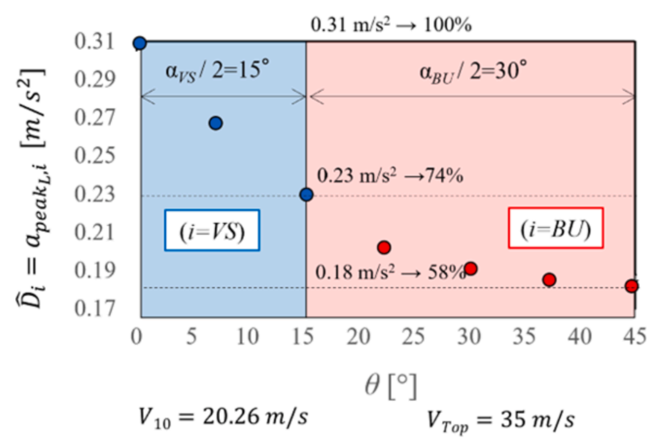

Fig. 11. Classification of the building response due to the arbitrary definition of the *VS* and *BU* sectors.

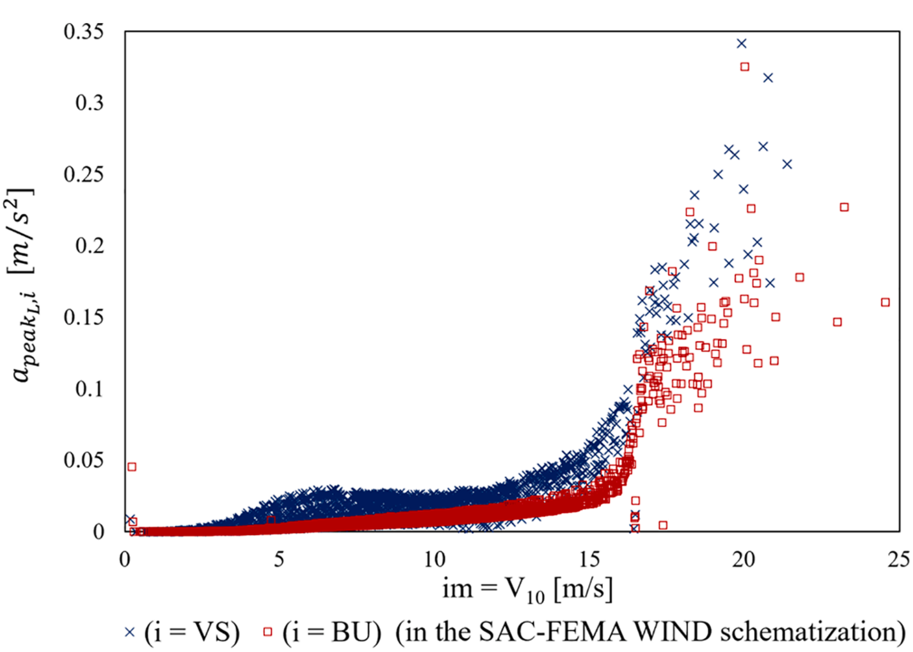

Fig. 10. Demand samples (MC analysis).

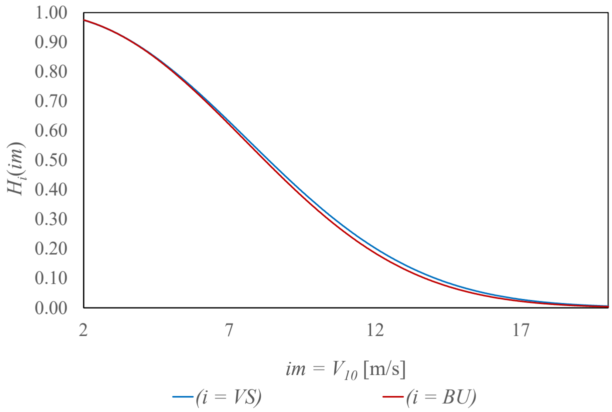

Fig. 12. Hazard curves for SAC-FEMA WIND.

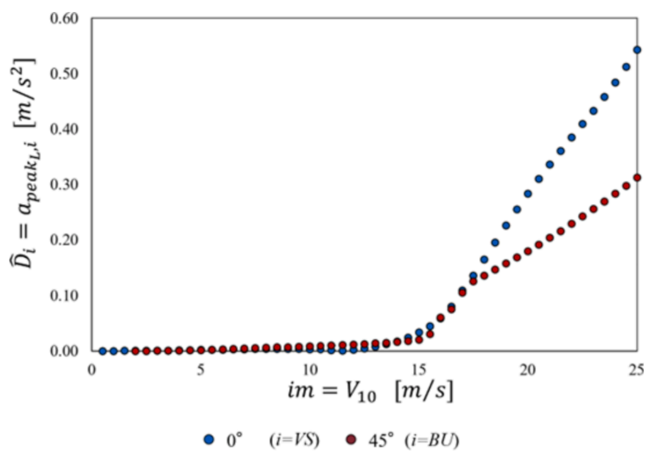

Fig. 13. Median Demand.

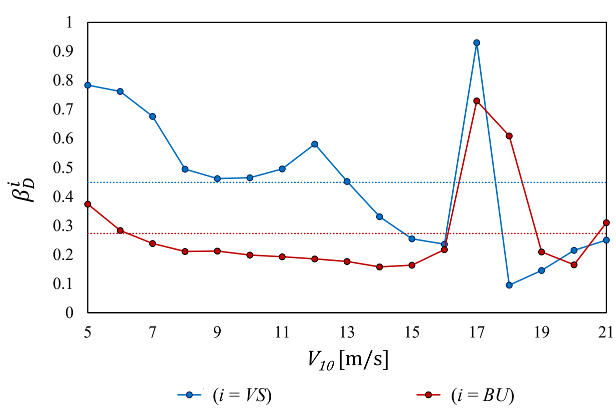

Fig. 14. Demand dispersions at different *IM* values.

$$\sigma_v = 0.75\sigma_u \tag{26}$$

$$\sigma_u^2 = [6 - 1.1\,arctan(ln(z_0) + 1.75\,)\,]\,u_*^2 \tag{27}$$

$$n_v(z_l) = \frac{nL_v(z_l)}{V_m(z_l)} \tag{28}$$

In addition to the symbols already defined above, u_* is the friction or shear velocity (in m/s), given by: $[(K)^{1/2}\,V_{10}]$, where K is a coefficient

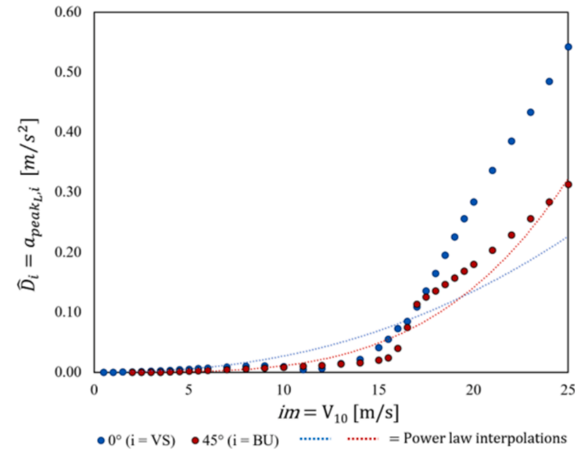

Fig. 15. Median demand basic interpolation.

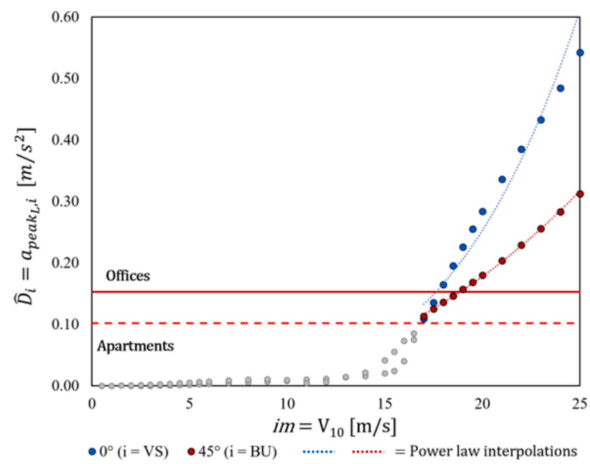

Fig. 16. Median demand improved interpolation.

Table 3
SAC-FEMA WIND parameters and obtained MAFs for *APT* case (it was P^{APT} MC = 0.026). Basic versus Improved interpolation of the median Demand.

Parameter	Basical median Demand interpolation Apartment building		Improved median Demand interpolation Apartment building	
	$i = VS$	$i = BU$	$i = VS$	$i = BU$
$V_{10,\ i,s}$ (m/s) hazard Eq. (31)	18.06; 15.66; 12.65	17.75; 16.32; 14.40	15.753; 14.20; 12.154	16.28; 14.776; 12.77
$k_{0,\ i}$, $k_{1,\ i}$ and $k_{2,\ i}$ hazard Eq. (6)	2.28e-18; −34.35; 7.51	1.504e-23; −43.33; 9.22	6.99e-14; −26.55; 6.039	3.0756e-17; −32.697; 7.28
$\widehat{C}^{APT}$ (m/s^2)	0.102		0.102	
$im^{\widehat{C}^{APT}}$ (m/s)	19.39	18.51	16.59	17.09
$H_i\left(im^{\widehat{C}^{APT}}\right)$ Eq. (6)	0.0084	0.0097	0.0349	0.0215
a_i; b_i demand Eq (2)	0.0056; 3.311	0.0022; 3.683	0.000295; 4.54	0.0126; 3.171
ϕ_i^{APT} Eq (9)	0.767	0.886	0.885	0.8793
q_i Eq (8)	0.784	0.908	0.8944	0.903
β_{D_i}	0.449	0.273	0.449	0.2723
β_C^{APT}	0.143	0.143	0.143	0.143
n_i Eq (13)	0.31	0.69	0.31	0.69
λ_i^{APT} Eq (7)	0.0164	0.0129	0.0426	0.0274
λ^{APT} Eq (13)	0.0140 (**-46.2% with respect to P^{APT} MC)**		0.0321 (**+23.5% with respect to P^{APT} MC)**	

Table 4
SAC-FEMA WIND parameters and obtained MAFs for *OFF* case (it was P^{OFF} MC = 0.011). Basic versus Improved interpolation of the median Demand.

Parameter	Basical median Demand interpolation Office building		Improved median Demand interpolation Office building	
	$i = VS$	$i = BU$	$i = VS$	$i = BU$
$V_{10,\ i\_s\_}$ (m/s) hazard Eq. (31)	20.415; 17.707; 14.304	19.814; 18.225; 16.08	17.225; 15.527; 13.289	18.503; 16.791; 14.515
$k_{0,\ i}$, $k_{1,\ i}$ and $k_{2,\ i}$ hazard Eq. (6)	1.33e-26; −47.98; 9.955	5.336e-33; −58.69; 11.93	3.555e-18; –33.94; 7.418	1.62e-25; −46.61; 9.815
$\widehat{C}^{OFF}$ (m/s^2)	0.153		0.153	
$im^{\widehat{C}^{OFF}}$ (m/s)	21.92	20.66	18.14	19.42
$H_i\left(im^{\widehat{C}^{OFF}}\right)$ Eq. (6)	0.0018	0.0025	0.0162	0.0056
a_i; b_i demand Eq (2)	0.0056; 3.311	0.0022; 3.683	2.954E-4; 4.54	0.0126; 3.1712
ϕ_i^{OFF} Eq (9)	0.719	0.867	0.8663	0.8542
q_i Eq (8)	0.732	0.884	0.8734	0.8732
β_{D_i}	0.449	0.273	0.449	0.273
β_C^{OFF}	0.114	0.114	0.114	0.114
n_i Eq (13)	0.31	0.69	0.31	0.69
λ_i^{OFF} Eq (7)	0.0054	0.0039	0.0219	0.0086
λ^{OFF} Eq (13)	0.0044 **(-60 % with respect to P^{OFF} MC)**		0.0127 **(+15.5% with respect to P^{OFF} MC)**	

depending on the roughness length z_0, the integral scale L_v (z_l) of the across-wind turbulent components are given in [47].

The cross-PSD terms (out of diagonal terms of the PSD floor forces matrix) are given by:

$$S^{TOT}{}_{F_{v_l}F_{v_k}}(n, z_l, z_k) = \sqrt{S^{TOT}{}_{F_{v_l}F_{v_l}}(n, z_l, z_l) \bullet S^{TOT}{}_{F_{v_k}F_{v_k}}(n, z_k, z_k)}\, exp\left(-f_{jk}(n)\right) \tag{29}$$

Where

$$f_{jk}(n) = \frac{|n|\, C_z \left|z_j - z_k\right|}{V_m\left(z_j\right) + V_m(z_k)} \tag{30}$$

And C_z is a coefficient inversely proportional to the spatial correlation of the process (decay coefficient), set equal to 6.5 ([47]).

The values of the combination coefficient $c(\theta)$ in Equation (18) have been calibrated to reproduce the across-wind top floor peak accelerations results obtained for a certain V_{10} and at various θ values by using time history forces determined from wind tunnel tests as already published in [4] and shown in Fig. 9.

The random parameters used in the MC analysis are shown in Table 2. Regarding the Hazard, V_{10} and θ are described, on an annual occurrence, by a joint probability density function that is obtained by assuming that the mean wind velocity for any given wind direction follows a Weibull distribution, and the interdependence of wind distribution in different wind directions can be reflected by the relative frequency of occurrence of wind. The shape and scale coefficient of the Weibull distributions are evaluated for 16 values of θ (between 0° and 360°) by the statistical data collected in the NIST® database http://www.itl.nist.gov/div898/winds/datasets.htm. The wind incidence angle θ has the relative frequency of occurrence derived by the wind velocity database. The roughness length z_0 is characterized by a lognormal PDF. The mean value μ_{z0} and the standard deviation σ_{z0} of z_0 are expressed as a function of θ considering four sectors: in the first one ($0^\circ < \theta < 45^\circ$ and $315^\circ < \theta < 0^\circ$), μ_{z0} is equal to 0.08 m; μ_{z0} is equal to 0.10 m in the second and third sector ($45^\circ < \theta < 135^\circ$ and for $225^\circ < \theta < 315^\circ$; and equal to 0.12 m in the fourth sector ($135^\circ < \theta < 225^\circ$). The value of COV_{z0} (coefficient of variation) is assumed equal to 0.30.

Regarding the structural system and the wind-structure interaction, the viscous damping ratio ξ is assumed to have a longnormal probability distribution function, with mean $\mu_\xi = 0.008$ and coefficient of variation $COV_\xi = 0.3$. The aerodynamic lift C_L coefficient is characterized by a Gaussian distribution. The mean value μ_{C_L} depend on the value of θ varying from that corresponding to a square shape (for $\theta = 0^\circ$) to that corresponding to a rhomboidal shape (for $\theta = 45^\circ$). The coefficient of variation of C_L varies between 0.05 and 0.10 for V_{10} varying between 0 and 25 m/s.

The results of the MC analysis in terms of structural demand samples are shown in Fig. 10, where different colors and symbols are used to indicate demand samples which comes from angles of incidence that, in the SAC-FEMA WIND formulation, are schematically associated to different response regimes (namely *BU* and *VS*) as detailed in previous and in the next sections.

As said above, capacity (perception thresholds) samples have been generated from LN distributions considering $\widehat{C}^{APT} = 0.101$ m/s^2, β_C^{APT}=0.143, $\widehat{C}^{OFF} = 0.153$ m/s^2 and$\beta_C^{OFF} = 0.114$.

The annual failure probabilities P^j obtained for the occupants' comfort SLS with reference to the different building occupations (j = *APT* or *OFF*) are: P^{APT} MC = 0.026 and P^{OFF} MC = 0.011.

4.1. Application of the SAC-FEMA WIND

The SAC-FEMA WIND method has been implemented for the case study as described in section 2.2 and 2.3. Regarding the hazard, as anticipated, all the possible wind incident angles have been grouped in two cases: the *VS* sectors (assumed to induce predominant *VS* response) having $\alpha_{VS} = 30^\circ$ amplitude (±15° with respect to $\theta = 0^\circ, 90^\circ, 180^\circ, 270^\circ$) and the *BU* sectors, for which $\alpha_{BU} = 60^\circ$ to be complementary to the previous. The choice of the α_{VS} and α_{BU} amplitudes is partially arbitrary and should be calibrated: in the present case judgment on the choice has been done on the basis of what shown in Fig. 11 (elaborated starting from Fig. 9 above), where the decrement of the median *D* with θ due to the transition between *VS* and *BU* response regimes is quantified for a certain *im*. The effects of changing the chosen values α_{VS} is discussed in the Appendix of the paper.

When α_{VS} and α_{BU} amplitudes are defined, they affect the n_{VS} and n_{BU} used in Equation (13), which are the annual probabilities at the site for the wind angle of incidence to fall in the sector associated to *VS* or to *BU* respectively. Given the above-mentioned values for the α_{VS} and α_{BU} amplitudes, it results $n_{VS} = 0.34$ and $n_{BU} = 0.66$.

The α_{VS} and α_{BU} amplitudes also determine the selection from the wind database of the Weibull shape and scale parameters values to be averaged in order to find the *VS* and *BU* hazard curves. In the present case, the two resulting hazard curves are almost identical and are shown in Fig. 12.

A biased-fit interpolation of the hazard has been conducted by using the following three abscissa values as interpolation points [51]:

$$V_{10,i\_s} = \left(\frac{V_{10}^{\widehat{C}^j}}{a_i}\right)^{1/b_i} exp\left(p_s \frac{\sqrt{\beta_{D,i}^2 + \beta_C^{j\,2}}}{b_i}\right) \tag{31}$$

Where $p_s = -0.5, -1.5, -3.0$ for $s = 1,2,3$, $i = VS$ or BU, $j = APT$ or *OFF*.

As said in Section 2, the median demand functions $\widehat{D}_i = \widehat{a}_{peak\_L,i}$ for $i = VS$ and BU (Fig. 13), have been obtained by a set of structural analyses at increasing *IM* values and by considering the mean/median values of the uncertain parameters listed in Table 2. On the other hand, the demand dispersions $\beta_{D,i}$ for $i = VS$ and BU can be obtained as dispersion of response samples from the previous MC results, where all the uncertain parameters vary under their assigned probabilistic distributions: the samples dispersions conditional to the *IM* values evaluated from MC, are shown in Fig. 14 for the two different *D* regimes and together with their average values, equal to $\beta_{D,VS} = 0.45$ and $\beta_{D,BU} = 0.25$ (dashed lines in Fig. 14), which are the *D* dispersion values used below in the MAF evaluation. It is worth noting that the demand dispersion appearing at 17 m/s in Fig. 14 does not have any physical meaning but is rather an outlier value due to the limited samples falling around that V_{10} value in the MC samples population.

As said above, on the capacity side (perception thresholds) the median and dispersion values considered are $\widehat{C}^{APT} = 0.101$ m/s^2, β_C^{APT}=0.143, $\widehat{C}^{OFF} = 0.153$ m/s^2 and$\beta_C^{OFF} = 0.114$.

One important point concerns the median demand interpolation. In order to maintain the consistency with the original SAC-FEMA approach, the power interpolation law shown in Equation (2) is used. This choice actually is not the best one for wind response demands due to the fact that the power law has to pass from the origin and, with respect to seismic induced demands, as already said, the tangent steepness to the curve, in the *im*-$\widehat{D}$ plane, increases rapidly with the increasing *IM* values. Due to this, if the whole *IM* range is considered for median *BU* and *VS* demand interpolation purposes, as shown in Fig. 15, the fitting is not adequate at large *IM* values (which are expected to provide the main contribute to the MAF), something leading to an unsatisfactory MAF estimation. To avoid this drawback, an “improved” median demand interpolation is proposed by considering a reduced *IM* values range for evaluating a_i and b_i, for both $i = VS$ and BU. By selecting, as *IM* minimum interpolation value, the one that corresponds to the lower perception threshold ($\widehat{D}_i = \widehat{C}^{APT}$; $i = VS$ and BU) for the building, the interpolation is really improved at higher $\widehat{D}_i$ values (see Fig. 16), something leading to a good approximation of the P^{APT} and P^{OFF} by the MAF estimated with the SAC-FEMA WIND.

With the goal of showing the importance of the improved interpolation, the obtained value of the parameters and the MAF obtained by its implementation are shown in tables 3 and 4 for $j = APT$ and $j = OFF$ respectively, and they are compared with the same values coming up by the “basic” interpolation where the whole *IM* range is considered. The obtained MAFs are also compared with the comfort SLS probabilities P^{APT} MC and P^{OFF} MC, obtained by the MC analysis, allowing a critical evaluation of the SAC-FEM procedure.

A satisfactory result for the MAF should be conservative with respect to the MC result, and it should differ no more than 25% from it, which is the uncertainty range considered as acceptable for failure probability estimations [81].

5. Discussion

From the results shown above, the following considerations can be made regarding the SAC-FEMA WIND method for MAFs evaluation in case of occupant’ comfort SLS:

- the differentiation between different aerodynamic response regimes for tall building (*VS* and *BU* in the examined case) is crucial for the correct schematization of the physic of the problem;
- the quality of the $\widehat{D}_i$ interpolation is also crucial for the correctness of the obtained MAFs. The proposed interpolation strategy for $\widehat{D}_i$, consisting in taking $im^{\widehat{C}^{APT}}$ as lower value of the *im* regression values interval, does lead to a satisfactory result for MAFs (in the sense specified above), while a full *im* interval for interpolation does not;

It is important to say that, even if it has been applied to the MAF evaluation for tall buildings occupants’ comfort SLS, the proposed SAC-FEMA WIND method has a general validity, and its extension to other LSs is straightforward and does not imply any change to the obtained format, by maintaining the differentiation between involved aerodynamic regimes. To use the SAC-FEMA WIND for the evaluation of the MAF of ULSs, all we need is choosing appropriate Demand and Capacity parameters, and using appropriate analysis techniques. For example, in case of ULSs related with the nonlinear inelastic response of wind-excited buildings, the peak IDR can be used as Demand parameter, and the incremental analyses for the evaluation of the median and the dispersion of the Demand can be implemented by nonlinear models in time domain, while the Capacity can be characterized by median and dispersion values already in use for earthquake analysis.

The application of the method to other structural typologies is also straightforward, since the chosen hazard *IM* is “structure independent” (is related only to the site climatology and not to structural features) and has general validity for all structural typologies. Obviously, appropriate analysis techniques and Demand/Capacity parameters must be selected for the investigated structural typologies and LS.

6. Conclusions

A novel SAC-FEMA WIND approach is proposed for Performance-Based assessment of structures under wind loads. Then it is applied to a 74-storey steel high-rise building to evaluate the Mean Annual Frequency (MAF) for the comfort serviceability limit state (SLS) in the across wind direction. The proposed approach is an extension to wind engineering problem of an already existing method, initially formulated for earthquakes. Such extension required the definition of detailed procedures to evaluate the effect of the wind incidence occurrence causing different response regimes (i.e. vortex shedding or buffeting). The SAC-FEMA WIND resulting MAF has been compared with the same SLS probability as obtained by a Monte Carlo simulation, showing satisfactory accordance and conservative estimation.

The development of the SAC-FEMA WIND method is an important step toward the next-generation Performance-Based Wind Engineering (PBWE) for structures. In fact, as already made in Earthquake Engineering, the definition Standards-oriented probabilistic PBE formats (like the one implemented in the SAC-FEMA WIND) will certainly increase the PBWE application in engineering practice.

In addition to the above, it is important to highlight that a certain uniformity of methods and formats for PBE of structures under different hazards, is one of the issues to address for the true implementation of Performance-Based Multi-Hazard Engineering (PB-MH-E) [48]: the SAC-FEMA WIND represents then a step forward the PB-MH-E of structures under wind and earthquakes.

The SAC-FEMA WIND method has been proposed here to specifically study the occupants’ comfort in tall buildings under wind. Further research is needed to:

- calibrate some of the analysis procedures and parameters used in the method. For example, a deeper investigation regarding the appropriate values for the parameters α_{VS} and α_{BU} defining the amplitude of the *VS* and *BU* sectors in the wind rose or regarding the

quantification of the capacity dispersion, by including the uncertainty in interpreting/quantifying the results of any given literature study to derive the LS capacity [77];
- applying the method to non-square floor buildings;
- applying the methos to the evaluation of MAFs of other Limit States.

Declaration of Competing Interest

The authors declare that they have no known competing financial interests or personal relationships that could have appeared to influence the work reported in this paper.

Data availability

Data will be made available on request.

Acknowledgments

Prof. Franco Bontempi from Sapienza University of Rome is gratefully acknowledged for the fruitful discussions regarding the paper. The financial support (grants ID No RP120172B79F3A52 and AR120172B863DEE9) received from Sapienza University by the authors is also gratefully aknowlwdged. The findings of this paper are part of the PhD thesis of the second author, developed under the tutoring of the first author.

Appendix

The effect of the α_{VS} amplitude on the resulting MAF has been investigated by comparing the result obtained for the evaluated MAFs by three different α_{VS} values: 20°, 30° (chosen value) and 40°. Fig. A1 (to be compared with Fig. 11 above) shows the different values in terms of response classification at varying θ values, while Tables A1 and A2 show the effects of different α_{VS} values on the computed MAFs and the parameters. It is evident that the uncertainties affecting the choice of α_{VS} slightly influences the final result, than the procedure can be declared as robust with respect to this uncertainty.

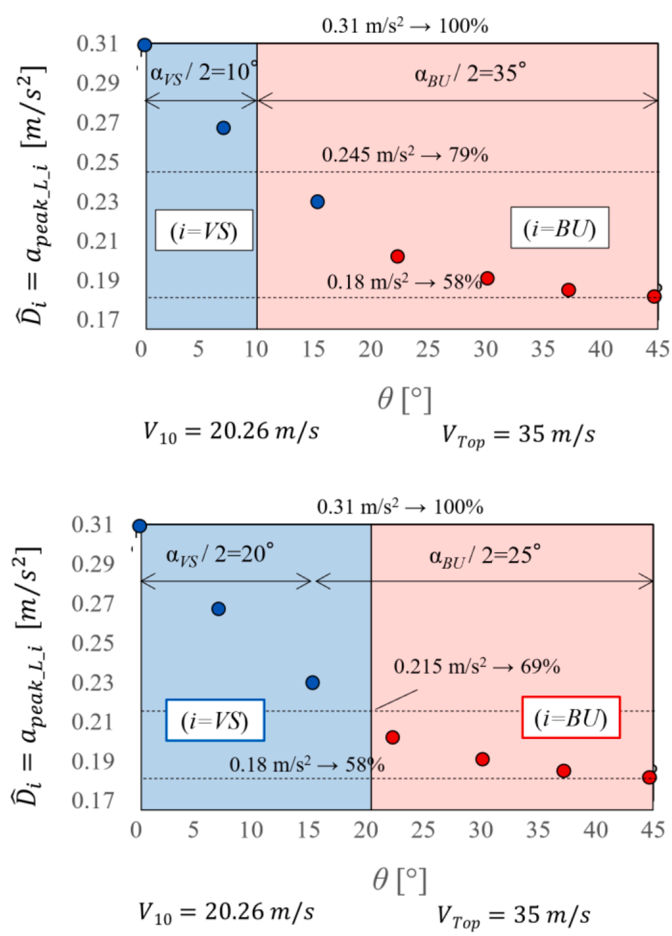

Fig. A1. Classification of the building response at different definition of the *VS* and *BU* sectors. $\alpha_{VS} = 20°$ (top) and $\alpha_{VS} = 40°$ (bottom).

Table A1
SAC-FEMA WIND parameters and obtained MAFs for *APT* case (it was P^{APT} MC = 0.026). Effect of different assumed values for alfa *VS*.

Parameter	Alfa $VS = 10$ Apartment building $i = VS$	$i = BU$	Alfa $VS = 15$ Apartment building $i = VS$	$i = BU$	Alfa $VS = 20$ Apartment building $i = VS$	$i = BU$
$V_{10,\ i,s\_}$ (m/s) hazard Eq. (31)	15.974; 14.805; 13.211	16.092; 14.237; 11.859	15.753; 14.20; 12.154	16.28; 14.776; 12.77	15.638; 13.891; 11.629	16.380; 15.044; 13.240
$k_{0,\ i}$, $k_{1,\ i}$ and $k_{2,\ i}$ hazard Eq. (6)	1.226e-15; −29.484; 6.562	4.215e-15; −29.005; 6.584	6.99e-14; −26.55; 6.039	3.0756e-17; −32.697; 7.28	6.264e-13; −24.913; 5.735	1.294e-18; −35.097; 7.734
$\widehat{C}^{APT}$ (m/s^2)	0.102		0.102		0.102	
$im^{\widehat{C}^{APT}}$ (m/s)	16.59	17.09	16.59	17.09	16.59	17.09
$H_i\left(im^{\widehat{C}^{APT}}\right)$ Eq. (6)	0.0372	0.022	0.0349	0.0215	0.0345	0.0207
a_i; b_i demand Eq (2)	2.954e-4; 4.54	0.0126; 3.171	0.000295; 4.54	0.0126; 3.171	2.954e-4; 4.54	0.0126; 3.171
ϕ_i^{APT} Eq (9)	0.9296	0.8364	0.885	0.8793	0.861	0.899
q_i Eq (8)	0.9410	0.8556	0.8944	0.903	0.8699	0.925
$\beta_{D,i}$	0.314	0.359	0.449	0.2723	0.519	0.229
β_C^{APT}	0.143	0.143	0.143	0.143	0.143	0.143
n_i Eq (13)	0.20	0.80	0.31	0.69	0.419	0.581
λ_i^{APT} Eq (7)	0.0415	0.0311	0.0426	0.0274	0.0441	0.0253
λ^{APT} Eq (13)	0.0332 (+**28% with respect to P^{APT} MC**)		0.0321 (**+23.5% with respect to P^{APT} MC**)		0.0332 (+**28% with respect to P^{APT} MC**)	

Table A2
SAC-FEMA WIND parameters and obtained MAFs for *OFF* case (it was P^{OFF} MC = 0.011). Effect of different assumed values for alfa *VS*.

Parameter	Alfa $VS = 10$ Office building $i = VS$	$i = BU$	Alfa $VS = 15$ Office building $i = VS$	$i = BU$	Alfa $VS = 20$ Office building $i = VS$	$i = BU$
$V_{10,\ i,s\_}$ (m/s) hazard Eq. (31)	17.466; 16.188; 14.445	18.276; 16.179; 13.476	17.225; 15.527; 13.289	18.503; 16.791; 14.515	17.099; 15.189; 12.716	18.615; 17.096; 15.046
$k_{0,\ i}$, $k_{1,\ i}$ and $k_{2,\ i}$ hazard Eq. (6)	1.779e-20; −37.659; 8.061	2.451e-22; −41.366; 8.874	3.555e-18; –33.94; 7.418	1.62e-25; −46.61; 9.815	6.411e-17; −31. 844; 7.041	1.3626e-27; −50.072; 10.445
$\widehat{C}^{OFF}$ (m/s^2)	0.153		0.153		0.153	
$im^{\widehat{C}^{OFF}}$ (m/s)	18.14	19.42	18.14	19.42	18.14	19.42
$H_i\left(im^{\widehat{C}^{OFF}}\right)$ Eq. (6)	0.0175	0.0058	0.0162	0.0056	0.0160	0.0053
a_i; b_i demand Eq (2)	2.954e-4; 4.54	0.0126; 3.1712	2.954E-4; 4.54	0.0126; 3.1712	2.954E-4; 4.54	0.0126; 3.1712
ϕ_i^{OFF} Eq (9)	0.9197	0.7996	0.8663	0.8542	0.8385	0.8802
q_i Eq (8)	0.9285	0.8147	0.8734	0.8732	0.8445	0.9018
$\beta_{D,i}$	0.314	0.359	0.449	0.273	0.519	0.229
β_C^{OFF}	0.114	0.114	0.114	0.114	0.088	0.088
n_i Eq (13)	0.20	0.80	0.31	0.69	0.419	0.581
λ_i^{OFF} Eq (7)	0.0206	0.0107	0.0219	0.0086	0.0232	0.0075
λ^{OFF} Eq (13)	0.0127 (+**15.5% with respect to P^{OFF} MC**)		0.0127 (+**15.5% with respect to P^{OFF} MC**)		0.0141 (+**28.2% with respect to P^{OFF} MC**)	

References

[1] Davenport AG. The relationship of reliability to wind loading. J Wind Eng Ind Aerod 1983;13(1–3):3–27. https://doi.org/10.1016/0167-6105(83)90125-3.

[2] Augusti G, Ciampoli M. Performance-Based Design in risk assessment and reduction. Prob Eng Mech 2008;23(4):496–508. https://doi.org/10.1016/j.probengmech.2008.01.007.

[3] Bezabeh MA, Bitsuamlak GT, Tesfamariam S. Performance based wind design of tall buildings: concepts, frameworks, and opportunities. Wind and Structures 2020; 31(2):103–42. https://doi.org/10.12989/was.2020.31.2.103.

[4] Ciampoli M, Petrini F, Augusti G. Performance-Based Wind Engineering: towards a general procedure. Struct Safety 2011;33(6):367–78. https://doi.org/10.1016/j.strusafe.2011.07.001.

[5] Smith MA, Caracoglia L. A Monte Carlo based method for the dynamic fragility analysis of tall buildings under turbulent wind loading. Eng Struct 2011;33(2): 410–20. https://doi.org/10.1016/j.engstruct.2010.10.024.

[6] Ciampoli M, Petrini F. Performance-based Aeolian risk assessment and reduction for tall buildings. Probab Eng Mech 2012;28:75–84. https://doi.org/10.1016/j.probengmech.2011.08.013.

[7] Petrini F, Ciampoli M. Performance-based wind design of tall buildings. Structure & Infrastructure Engineering - Maintenance, Management, Life-Cycle Design & Performance 2012;8(10):954–66. https://doi.org/10.1080/15732479.2011.574815.

[8] Barbato M, Petrini F, Unnikrishnan VU, Ciampoli M. Performance-Based Hurricane Engineering (PBHE) framework. Struct Safety 2013;45:24–35. https://doi.org/10.1016/j.strusafe.2013.07.002.

[9] Spence SMJ, Kareem A. Performance-based design and optimization of uncertain wind-excited dynamic building systems. Eng Struct 2014;78:133–44. https://doi.org/10.1016/j.engstruct.2014.07.026.

[10] Bernardini E, Spence SMJ, Kwon D-K, Kareem A. Performance-Based Design of High-Rise Buildings for Occupant Comfort. J Struct Eng 2015;141(10):04014244. https://doi.org/10.1061/(ASCE)ST.1943-541X.0001223.

[11] Cui W, Caracoglia L. Simulation and analysis of intervention costs due to wind-induced damage on tall buildings. Eng Struct 2015;87:183–97. https://doi.org/10.1016/j.engstruct.2015.01.001.
[12] Tabbuso P, Spence SMJ, Palizzolo L, Pirrotta A, Kareem A. An efficient framework for the elasto-plastic reliability assessment of uncertain wind excited systems. Struct Safety 2016;58:69–78. https://doi.org/10.1016/j.strusafe.2015.09.001.
[13] Chuang WC, Spence SMJ. A performance-based design framework for the integrated collapse and non-collapse assessment of wind excited buildings. Eng Struct 2017;150:746–58. https://doi.org/10.1016/j.engstruct.2017.07.030.
[14] Ierimonti L, Caracoglia L, Venanzi I, Materazzi LA. Investigation on life-cycle damage cost of wind-excited tall buildings considering directionality effects. J Wind Eng Ind Aerod 2017;171:207–18. https://doi.org/10.1016/j.jweia.2017.09.020.
[15] Tessari RK, Kroetz HM, Beck AT. Performance-based design of steel towers subject to wind action. Engin Struct 2017;143:549–57. https://doi.org/10.1016/j.engstruct.2017.03.053.
[16] Cui W, Caracoglia L. A unified framework for performance-based wind engineering of tall buildings in hurricane-prone regions based on lifetime intervention-cost estimation. Struct Safety 2018;73:75–86. https://doi.org/10.1016/j.strusafe.2018.02.003.
[17] Fu J, Zheng Q, Huang Y, Wua J, Pi Y, Liu Q. Design optimization on high-rise buildings considering occupant comfort reliability and joint distribution of wind speed and direction. Engin Struct 2018;156:460–71. https://doi.org/10.1016/j.engstruct.2017.11.041.
[18] Spence SMJ. Optimization of uncertain and dynamic high-rise structures for occupant comfort: An adaptive kriging approach. Struct Safety 2018;75:57–66. https://doi.org/10.1016/j.strusafe.2018.05.008.
[19] Caracoglia L. Unified stochastic dynamic and damage cost model for the structural analysis of tall buildings in thunderstorm-like winds. ASCE-ASME J. Uncertain. Eng Syst, Part A: Civil Eng. 2018;4(4):04018043. https://doi.org/10.1061/AJRUA6.0000999.
[20] Bezabeh MA, Bitsuamlak GT, Popovski M, Tesfamariam S. Probabilistic serviceability-performance assessment of tall mass-timber buildings subjected to stochastic wind loads: part I-structural design and wind tunnel testing. J Wind Eng Ind Aerod 2018;181:85–103. https://doi.org/10.1016/j.jweia.2018.08.012.
[21] Bezabeh MA, Bitsuamlak GT, Popovski M, Tesfamariam S. Probabilistic serviceability-performance assessment of tall mass-timber buildings subjected to stochastic wind loads: part II- structural reliability analysis. J Wind Eng Ind Aerod 2018;181:112–25. https://doi.org/10.1016/j.jweia.2018.08.013.
[22] Chuang W-C, Spence SMJ. An efficient framework for the inelastic performance assessment of structural systems subject to stochastic wind loads. Eng Struct 2019; 179:92–105. https://doi.org/10.1016/j.engstruct.2018.10.039.
[23] Suksuwan A, Spence SMJ. Performance-based design optimization of uncertain wind excited systems under system-level loss constraints. Struct Safety 2019;80: 13–31. https://doi.org/10.1016/j.strusafe.2019.03.004.
[24] Suksuwan A, Spence SMJ. Performance-based bi-objective design optimization of wind-excited building systems. J Wind Eng Ind Aerod 2019;190:40–52. https://doi.org/10.1016/j.jweia.2019.03.028.
[25] Cui W, Caracoglia L. Performance-based wind engineering of tall buildings examining life-cycle downtime and multisource wind damage. J Struct Eng 2020; 146(1):04019179. https://doi.org/10.1061/(ASCE)ST.1943-541X.0002479.
[26] Cui W, Ma T, Caracoglia L. Time-cost ‘‘trade-off’’ analysis for wind-induced inhabitability of tall buildings equipped with tuned mass dampers. J Wind Eng Ind Aerod 2020;207:104394. https://doi.org/10.1016/j.jweia.2020.104394.
[27] Petrini F, Giaralis A, Wang Z. Optimal tuned mass-damper-inerter (TMDI) design in wind-excited tall buildings for occupants' comfort serviceability performance and energy harvesting. Eng Struct 2020;204:109904. https://doi.org/10.1016/j.engstruct.2019.109904.
[28] Elezaby F, El Damatty A. Ductility based design approach of tall buildings under wind loads. Wind and Structures 2020;31(2):143–52. https://doi.org/10.12989/was.2020.31.2.143.
[29] Ouyang Z, Spence SMJ. A Performance-Based Wind Engineering Framework for Envelope Systems of Engineered Buildings Subject to Directional Wind and Rain Hazards. J Struct Eng 2020;146(5):04020049. https://doi.org/10.1061/(ASCE)ST.1943-541X.0002568.
[30] Ouyang Z, Spence SMJ. Performance-based wind-induced structural and envelope damage assessment of engineered buildings through nonlinear dynamic analysis. J Wind Eng Ind Aerod 2021;208:104452. https://doi.org/10.1016/j.jweia.2020.104452.
[31] Zhang L, Caracoglia L. Layered Stochastic Approximation Monte-Carlo method for tall building and tower fragility in mixed wind load climates. Eng Struct 2021;239: 112159. https://doi.org/10.1016/j.engstruct.2021.112159.
[32] Đepina I, Divić V, Munjiza A, Peroš B. Perfomance-based wind engineering assessment of critical telecommunication infrastructure subjected to bora wind. Eng Struct 2021;236:112083. https://doi.org/10.1016/j.engstruct.2021.112083.
[33] Merhi A, Letchford CW. Computational method in database-assisted design for wind engineering with varying performance objectives. Wind and Structures 2021; 32(5):439–52. https://doi.org/10.12989/was.2021.32.5.439.
[34] Chuang W-C, Spence SMJ. A framework for the efficient reliability assessment of inelastic wind excited structures at dynamic shakedown. J Wind Eng Ind Aerod 2022;220:104834. https://doi.org/10.1016/j.jweia.2021.104834.
[35] Dimitrios V. Bilionis DV, Vlachakis K, Dimitrios Vamvatsikos D, Dasiou ME, Vayas I, Lagouvardos K. Risk Assessment of Rehabilitation Strategies for Steel Lattice Telecommunication Towers of Greece under Extreme Wind Hazard. Eng Structures. In press.
[36] Kareem A. Emerging frontiers in wind engineering: Computing, stochastics, machine learning and beyond. J Wind Eng Ind Aerod 2020;206:104320. https://doi.org/10.1016/j.jweia.2020.104320.
[37] Spence SMJ, Lombardo FT, McCormick JP. Recent Advances in the Modeling of Wind Hazards and Performance Assessment of Wind-Excited Systems. J. Struct. Eng., 2022, 148(2): 02021003. Special issue foreword. https://doi.org/10.1061/(ASCE)ST.1943-541X.0003258.
[38] Fragiadakis M, Vamvatsikos D, Karlaftis MG, Lagaros ND, Papadrakakis M. Seismic assessment of structures and lifelines. J Sound Vib 2015;334:29–56. https://doi.org/10.1016/j.jsv.2013.12.031.
[39] Olmati P, Petrini F, Vamvatsikos D, Gantes CJ. Simplified fragility-based risk analysis for impulse governed blast loading scenarios. Eng Struct 2016;117: 457–69. https://10.1016/j.engstruct.2016.01.039.
[40] Nakai M, Hirakawa K, Yamanaka M, Okuda H, Konishi A. Performance-based wind-resistant design for high-rise structures in Japan. Int J High-Rise Build 2013;2(3): 271–83. https://doi.org/10.21022/IJHRB.2013.2.3.271.
[41] Mohammadi A, Azizinamini A, Griffis L, Irwin P. Performance assessment of an existing 47-story high-rise building under extreme wind loads. J Struct Eng 2019; 145(1):04018232. https://doi.org/10.1061/(ASCE)ST.1943-541X.0002239.
[42] Micheli L, Alipour A, Laflamme S, Sarkar P. Performance-based design with life-cycle cost assessment for damping systems integrated in wind excited tall buildings. Eng Struct 2019;195:438–51. https://doi.org/10.1016/j.engstruct.2019.04.009.
[43] Hart GC, Jain A. Performance-based wind evaluation and strengthening of existing tall concrete buildings in the Los Angeles region: dampers, nonlinear time history analysis and structural reliability. Struct Des Tall Spec Build 2014;23(16):1256–74. https://doi.org/10.1002/tal.1139.
[44] Pozos-Estrada A. A simple procedure to evaluate the wind induced acceleration in tall buildings: an application to Mexico. Wind and Structures 2018;27(5):337–45. https://doi.org/10.12989/was.2018.27.5.337.
[45] Cornell AC, Jalayer F, Hamburger RO, Foutch DA. Probabilistic basis for 2000 SAC Federal Emergency Management Agency steel moment frame guidelines. J Struct Eng 2002;128(4):526–33.
[46] ASCE/SEI (ASCE/Structural Engineering Institute). Pre-standard for Performance-Based Wind Design. Reston, VA, U.S.A.: American Society of Civil Engineers; 2019.
[47] CNR-DT 207/2008. Guide for the Assessment of Wind Actions and Effects on Structures. Rome, Italy: National Research Council of Italy; 2010.
[48] Petrini F, Gkoumas K, Rossi C, Bontempi F. Multi-Hazard Assessment of Bridges in Case of Hazard Chain: State of Play and Application to Vehicle-Pier Collision Followed by Fire. Frontiers in Built Environment - Bridge Engineering 2020. https://doi.org/10.3389/fbuil.2020.580854.
[49] Vamvatsikos D. Derivation of new SAC/FEMA performance evaluation solutions with second-order hazard approximation. Earthquake Engng Struct Dyn 2013;42: 1171–88. https://doi.org/10.1002/eqe.2265.
[50] Franchin P, Petrini F, Mollaioli F. Improved risk-targeted performance-based seismic design of reinforced concrete frame structures. Earthquake Engng Struct Dyn 2018;47(1):49–67. https://doi.org/10.1002/eqe.2936.
[51] Vamvatsikos D. Accurate Application and Second-Order Improvement of SAC/FEMA Probabilistic Formats for Seismic Performance Assessment. J Struct Eng 2014;140(2):04013058. https://doi.org/10.1061/(ASCE)ST.1943-541X.0000774.
[52] Dolsek M, Fajfar P. The effect of masonry infills on the seismic response of a four-storey Reinforced concrete frame—A probabilistic assessment. Eng Struct 2008;30 (11):3186–92. https://doi.org/10.1016/j.engstruct.2008.04.031.
[53] Vamvatsikos D, Allin Cornell CA. Incremental dynamic analysis. J Earthq Eng Struct Dyn 2002;31(3):491–514. https://doi.org/10.1002/eqe.141.
[54] Bradley BA. Practice-oriented estimation of the seismic demand hazard using ground motions at few intensity levels. Earthq Eng Struct Dyn 2013;42:2167–85. https://doi.org/10.1002/eqe.2319.
[55] Davies A, Gaisworthy JK, Gibbons M, Irwin PA, Morava B, Sifton V, et al. Wind Engineering for Tall and Supertall Buildings. In: Tamboli AR, editor. Tall and Supertall Buildings, planning and design. New York: MC Graw Hill Education; 2014. p. 289–360.
[56] Sharma A, Mittal H, Gairola A. Mitigation of wind load on tall buildings through aerodynamic modifications: Review. J of Build Eng 2018;18:180–94. https://doi.org/10.1016/j.jobe.2018.03.005.
[57] Tamura T, Miyagi T, Kitagishi T. Numerical prediction of unsteady pressures on a square cylinder with various corner shapes. J Wind Eng Ind Aerodyn 1998;74: 531–42. https://doi.org/10.1016/S0167-6105(98)00048-8.
[58] Li Y-G, Yan J-H, Li Y, Xiao C-X, JMa J-X. Wind tunnel study of wind effects on 90∘ helical and square tall buildings: A comparative study. Journal of Building Engineering 2021;42:103068. https://doi.org/10.1016/j.jobe.2021.103068.
[59] Taranath SB. Structural Analysis and Design of Tall Buildings. Steel and Composite Construction. Taylor & Francis Group Boca Raton, FL, USA: CRC Press; 2012.
[60] Burton MD, Kwok KCS, Hitchcock PA, Denoon RO. Frequency dependence of human response to wind-induced building motion. J Struct Eng 2006;132(2): 296–303. https://doi.org/10.1061/(ASCE)0733-9445(2006)132:2(296).
[61] Kwok KCS, Hitchcock PA, Burton MD. Perception of vibration and occupant comfort in wind-excited tall buildings. J Wind Eng Ind Aerodyn 2009;97(7–8): 368–80. https://doi.org/10.1016/j.jweia.2009.05.006.
[62] Lamb S, Kwok KCS, Walton D. Occupant comfort in wind-excited tall buildings: Motion sickness, compensatory behaviours and complaint. J Wind Eng Ind Aerodyn 2013;119:1–12. https://doi.org/10.1016/j.jweia.2013.05.004.
[63] Chen PW, Robertson LE. Human Perception Thresholds of Horizontal Motion. J. Struct. Div., ASCE 1972; 98(ST8), Proc. Paper 9142, 1681–1695.
[64] Iso. 6897. Guidelines for the Evaluation of the Response of Occupants of Fixed Structures, Especially Buildings and Offshore Structures, to Low-Frequency

Horizontal Motion (0.063 to 1 Hz). Geneva, Switzerland: International Organization for Standardization; 1984.
[65] Melbourne WH, Cheung JCK. Designing for serviceable accelerations in tall buildings. In: Proceedings of Fourth International Conference on Tall Buildings: 148–155. Hong Kong and Shanghai. 1988.
[66] Tamura Y, Fujii K, Sato T, Wakahara T, Kosugi M. Wind-induced vibration of tall towers and practical applications of tuned sloshing damper. Proceedings, 1, Symposium/Workshop on Serviceability of Buildings (Movements, Deformations, Vibrations): 228-241. Ottawa, Canada, 1988.
[67] NBR6123. Forças devidas ao vento em edificações. Associação Brasileira de Normas Técnicas, Rio de Janeiro, Brasil. 1988.
[68] Isyumov N. Criteria for acceptable wind-induced motions of tall buildings. *CTBUH Conf., Council on Tall Buildings and Urban Habitat*: 411-423. Chicago. 1993.
[69] Kanda J, Tamura Y, Fujii K, Ohtsuki T, Shioya K, Nakata S. Probabilistic Evaluation of Human Perception Threshold of Horizontal Vibration of Buildings (0.125 Hz to 6.0 H z). ASCE Structures Congress and the IASS International Symposium, Atlanta. 1994.
[70] Architectural Institute of Japan (AIJ). Guidelines for the evaluation of habitability to building vibration. AIJ-GEH-2004, Maruzen, Tokyo. 2004.
[71] Tamura Y, Kawana S, Nakamura O, Kanda J, Nakata S. Evaluation perception of wind-induced vibration in buildings. Proc Inst Civ Eng Struct Build 2006;159(SB5): 283–93. https://doi.org/10.1680/stbu.2006.159.5.283.
[72] ISO 10137. Bases for Design of Structures – Serviceability of Buildings and Walkways Against Vibrations. Geneva (Switzerland), International Organization for Standardization. 2007.
[73] Burton MD, Kwok KCS, Hitchcock PA. Occupant comfort criteria for wind-excited buildings: based on motion duration 2007;vol. 1.
[74] Sarkisian MP. Designing Tall Buildings Structure as Architecture. New York: Routledge; 2012.
[75] Ferrareto JO, França RLS, Mazzilli CEN. The impact of comfort assessment criteria on building design. In: Proceedings of the Council of Tall Buildings and Urban Habitat (CTBUH) – Future Cities, Towards Sustained Vertical Urbanism. Shanghai 2014:722–730.
[76] Pinto PE, Giannini R, Franchin P. Seismic Reliability Analysis of Structures. Pavia, Italy: IUSS Press; 2004.
[77] Yun S-Y, Hamburger RO, Cornell CA, Foutch DA. Seismic Performance Evaluation for Steel Moment Frames. J of Struct Eng 2002;128(4):534–45. https://doi.org/10.1061/(ASCE)0733-9445(2002)128:4(534).
[78] Vanmarke E. On the distribution of the first-passage time for normal stationary random processes. J Appl Mech 1975;42:215–20.
[79] Huang G, Chen X, Li M, Peng L. Extreme value of wind-excited response considering influence of bandwidth. J Mod Transport 2013;21(2):125–34. https://doi.org/10.1007/s40534-013-0015-x.
[80] Liang S, Liu S, Li QS, Zhang L, Gu M. Mathematical model of across-wind dynamic loads on rectangular tall buildings. J Wind Eng Ind Aerodyn 2002;90(12–15):1757–70.
[81] Iervolino I. Assessing uncertainty of estimation in PBEE. Earthq Eng Struct Dyn 2017;46(10):1711–23. https://doi.org/10.1002/eqe.2883.